Asociación Argentina
de Mecánica Computacional

Mecánica Computacional Vol XLII, pp. 363-372
A. Caggiano, G. Etse, P. Folino, M. Goldschmit, M. Pucheta, M. Storti (Eds.)
L. Battaglia, H. Castro, M. Coussirat, R. Paz, S. Sarraf, A. Scarabino (Issue eds.)
Buenos Aires, November 11-14, 2025

BOUNDARY LAYER DEVELOPMENT AND TRANSITION IN AIRFOILS AND FLAT PLATES: A COMPARATIVE STUDY

Franco L. Cortes[a,b] **and Santiago Márquez Damián**[a,b]

[a]*Centro de Investigación de Métodos Computacionales (CIMEC-CONICET/UNL), Predio Dr. Alberto Cassano, Colectora Ruta Nac. Nº 168, Km. 0, Paraje El Pozo, Santa Fe, Argentina,*
https://santafe.conicet.gov.ar/cimec/

[b]*Universidad Tecnológica Nacional, FRSF, Lavaise 610, Santa Fe, Argentina,*
http://www.frsf.utn.edu.ar/

Keywords: Laminar-turbulent transition, k–ω Models, Turbulent Flat plate, Airfoil (NACA0025).

Abstract. Accurate prediction of the laminar-to-turbulent transition remains one of the most significant challenges in flow simulations using turbulence models. This work focuses on the analysis of currently available transition models and their main limitations, particularly in flat plate and airfoil configurations. Boundary layer transition strongly influences the distribution of skin friction coefficient on flat plates, as well as pressure and lift coefficients on airfoils, playing a key role in predicting drag, losses, and aerodynamic efficiency. Various modeling approaches are reviewed, including correlation-based methods and modified versions of the k–omega SST model tailored to capture transition mechanisms. Despite their progress, many of these models show limitations when dealing with non-ideal boundary conditions, adverse pressure gradients, or varying levels of incoming turbulence. This study presents a numerical evaluation of transition models applied to flat plate flows, comparing the resulting skin friction distributions with experimental correlations. The work is then extended to airfoil simulations, analyzing the behavior of pressure and lift coefficients and their sensitivity to transition location and flow separation. This enables the analysis of boundary layer development and the effects of early or delayed transition on surface pressure distribution.The results indicate that while current models offer reasonable approximations under specific conditions, their generalization capability is still limited. It is concluded that further improvement is needed in the physical representation of transition mechanisms, along with more robust calibration under varied conditions, particularly for aerodynamic engineering applications.

ISSN: 2591-3522 DOI: 10.70567/mc.v42.ocsid8340

1 INTRODUCTION

The prediction of laminar-to-turbulent transition in aerodynamic flows represents one of the major challenges in computational fluid dynamics (CFD). This process involves the evolution of an initially laminar boundary layer into a turbulent state, with a significant increase in mixing and momentum transport. Its relevance in engineering lies in its direct influence on drag, lift, and the efficiency of aeronautical systems, turbomachinery, and hydraulic devices. An accurate estimation of the location and extent of transition is crucial for aerodynamic design, airfoil optimization, and flow control in industrial applications (Anderson, 2010; Menter et al., 2006).

In flat plates, transition has been extensively studied since the seminal works of Blasius (1907) and Schlichting and Gersten (2016), which provide empirical correlations for boundary layer development and the skin-friction coefficient (C_f). In the absence of pressure gradients, Blasius theory predicts the laminar thickness and $C_f \approx 0.664/\sqrt{Re_x}$, with a typical transition occurring at $Re_x \approx 3\times10^5$–5×10^5. The exact location of the transition varies with the intensity of the inlet turbulence.

For airfoils, flow complexity increases due to the combined effects of adverse pressure gradients and curvature. These conditions directly affect the transition process, influencing the pressure coefficient (C_p) distribution and, consequently, the prediction of lift and drag. Additionally, the possibility of laminar separation induced by adverse gradients poses a further challenge for numerical modeling (Ziadé et al., 2018; Langtry et al., 2004).

Although DNS (Direct Numerical Simulation) and LES (Large Eddy Simulation) capture transition and small-scale turbulent structures, their high computational cost makes them impractical for complex engineering problems or high Reynolds. Therefore, RANS (Reynolds-Averaged Navier-Stokes) models based on empirical correlations and transport equations are preferred, sacrificing physical resolution for computational efficiency (Pope, 2001).

This study assesses widely used RANS transition models: the four-equation k-ω SST LM (Langtry et al., 2004), the three-equation k-ω-γ SST variant (Menter et al., 2015), and two two-equation variants with boundary layer corrections, k-ω LowRe (Wilcox, 1992) and k-ω SST Modified (Cortes and Marquez Damián, 2024). The assessment is carried out through OpenFOAM simulations, comparing their performance in flat plate cases (T3 series ERCOFTAC (1995)) and airfoils (NACA0025 at $Re_c = 10^5$ (Ziadé et al., 2018)), validated against experimental data.

2 BOUNDARY LAYER EVOLUTION: TRANSITION REGIONS ON A FLAT PLATE

In flow over a flat plate with laminar inflow conditions, the transition to a turbulent regime does not occur abruptly but develops gradually along the streamwise coordinate x. Consequently, the boundary layer can be conceptually divided into three main regions, reflecting the progressive change in turbulence dynamics and velocity profile, as illustrated in Fig. 1.

2.1 Laminar Region

For low local Reynolds numbers ($Re_x = U_\infty x/\nu$), the flow remains laminar, with minimal Tollmien–Schlichting instabilities and turbulent viscosity $\nu_t \approx 0$. The velocity profile $U(y)$ follows the Blasius solution, exhibiting a steep wall gradient and a skin-friction coefficient governed by the equation $C_f(x) = 0.664/\sqrt{Re_x}$ (Blasius, 1907).

2.2 Transition Region

As Re_x increases, initial disturbances amplify intermittent structures (Tollmien–Schlichting instabilities), mixing turbulent spots with laminar remnants near the wall. Turbulent viscosity emerges ($\nu_t > 0$), causing the Blasius profile to deviate into a shape with logarithmic curvature in the mid-region. Turbulent transport reduces the wall gradient, increasing wall shear stress τ_w and C_f above the laminar correlation.

2.3 Fully Developed Turbulent Regime

The boundary layer balances turbulent production and dissipation, organizing the dimensionless velocity profile $U^+(y^+)$ into three subregions (Cortes and Marquez Damián, 2023, 2024):

- Viscous sublayer ($y^+ < 5$): dominated by molecular diffusion.
- Buffer region ($5 < y^+ < 30$): bridge between molecular and turbulent diffusion.
- Logarithmic region ($y^+ > 30$): governed by $U^+ = 1/\kappa \ln y^+ + B$, with $\kappa = 0.41$ (von Kármán constant) and $B \approx 5$ (integration constant).

The skin-friction coefficient follows Schlichting's correlation: $C_f(x) = 0.0592/Re_x^{1/5}$.

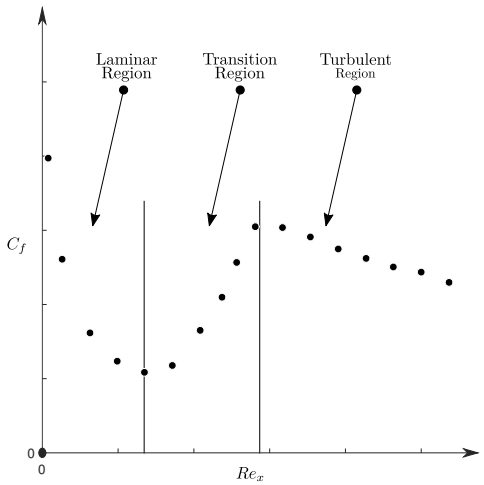

Figure 1: Division of regions in the evolution of C_f versus Re_x for a flat plate

3 CODE IMPLEMENTATION

This work employed OpenFOAM+ v2212 for computational fluid dynamics simulations, which natively includes the k-ω SSTLM transition model (Langtry et al., 2004). Additional in-house implementations were developed: k-ω SSTLowRe (Cortes and Marquez Damián, 2024), k-ω LowRe (Cortes and Marquez Damián, 2023), and k-ω-γ SST (Menter et al., 2015), the latter based on the code available in Fürst (2023) for reproducibility.

The simulations utilized a semi-implicit pressure-velocity coupling algorithm to ensure numerical stability. Spatial discretization employed second-order accurate schemes: linear interpolation for gradients, bounded upwind-biased schemes for velocity convection, limited linear schemes for turbulent variables (turbulence kinetic energy (k), Intermittency (γ_{Int}), Momentum Thickness Reynolds Number (Re_θ)), and first-order upwind for the specific dissipation rate (ω). Diffusion terms were discretized with a corrected linear scheme, and face-normal interpolations used linear methods with appropriate corrections.

The flat-plate configurations were resolved under steady-state conditions, while the airfoil cases were simulated in a transient regime, enhancing stability in refined meshes. Convergence was ensured by driving velocity and pressure residuals below 1×10^{-7}.

The comparative evaluation was carried out keeping the same spatial discretization, structured meshes and boundaryS conditions for all k-ω models, to isolate the turbulence model's effect on predictions. All implementations were verified through standard reference cases, ensuring reproducibility within the OpenFOAM+ platform.

4 APPLICATION OF THE PROPOSED MODELS

To evaluate the implemented models, reference test cases widely documented in the literature and recognized experimental databases were employed. These allow for the validation of the models' ability to predict transition under controlled conditions, ranging from simple flows to more complex cases with separation. The first benchmark considered was the ERCOFTAC T3 series (Ryhming, 1990), a standardized database compiling experimental data on laminar–turbulent transition under varying levels of free-stream turbulence and pressure gradients.

The flat-plate cases correspond to the T3A, T3AM, and T3B configurations, characterized by a plate with a rounded leading edge. This simple geometry is ideal for studying boundary-layer development without curvature effects, focusing on how the free-stream turbulence intensity (Tu) influences the onset of transition. The mesh used, obtained from the public GitHub-GammaSST repository (Fürst, 2023), was designed to validate models such as k-ω SSTLM and γ SST, with dimensions enabling the reproduction of initial laminar separation and its evolution toward turbulence, while matching experimental velocities.

Properties	**T3AM**	**T3A**	**T3B**	**NACA0025**
U_∞ [m/s]	19.8	5.18	9.4	5.0
k [m^2/s^2]	0.048	0.044	0.56	2.4×10^{-5}
ϵ [m^2/s^3]	1.4	0.947	20.90	3.5×10^{-5}
ω [1/s]	326.57	240.29	414.79	16.33
Tu [%]	0.9	3.3	6.5	0.8
L_t [m]	6.7×10^{-4}	8.7×10^{-4}	1.8×10^{-3}	3×10^{-4}
ν [m^2/s]	1.5×10^{-5}	1.5×10^{-5}	1.5×10^{-5}	1.5×10^{-5}
μ_t/μ	9.723	12.16	90.0	0.098

Table 1: Flow and turbulence properties for the evaluated cases, including freestream velocity (U_∞), turbulent kinetic energy (k), turbulent dissipation rate (ϵ), specific dissipation rate (ω), turbulence intensity (Tu), turbulent length scale (L_t), kinematic viscosity (ν), and turbulent-to-molecular viscosity ratio (μ_t/μ).

Additionally, the symmetric NACA0025 airfoil was evaluated, a well-established benchmark for low Reynolds number (Re_c) aerodynamic flows. Operating at an angle of attack (AOA) of 5° and $Re_c = 10^5$, with a chord length of $c = 0.3\,\text{m}$, this case introduces complexity due to adverse pressure gradients on the suction side, which promote laminar separation, reducing lift and increasing drag. Experimental and large eddy simulation (LES) data from Ziadé et al. (2018) provide measurements of the pressure coefficient (C_p), transition points, and velocity profiles, enabling comprehensive validation of the models' ability to capture these effects.

The combination of these cases—one geometrically simple (flat plate) and the other with curvature and AOA (airfoil)—enables a comprehensive assessment of the robustness and generality of the models.

4.1 Turbulent Flat Plate

This case represents a fundamental scenario for studying transition in the absence of pressure gradients, where the local Reynolds number and inlet turbulence intensity (Tu) determine the onset of turbulence. The T3A, T3AM, and T3B configurations vary Tu from 0.9% to 6.5%, allowing analysis of how external perturbations accelerate or delay transition compared to empirical correlations such as Blasius (laminar) and Schlichting (turbulent). As previously described, the meshes from the GitHub-GammaSST repository (Fürst, 2023), specifically designed for the initial validation of k-ω SSTLM and γ SST, were used (see Fig. 2).

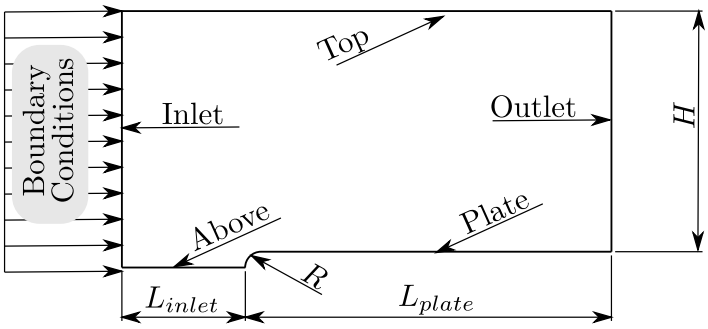

Figure 2: Schematic of the flat-plate geometry, including general boundary conditions (Inlet with U_∞, Outlet, Top and Above symmetric; $R = 7.5$ mm, $L_{inlet} = 0.04$ m, $L_{plate} = 3$ m, $H = 1$ m).

Patch	$\vec{U}$ [m/s]	k [m^2/s^2]	ω [1/s]	ν_t [m^2/s]	p [m^2/s^2]
Plate	$(0,0,0)$	0	OWF	0	$\vec{\nabla}p \cdot \vec{n} = 0$
Top	$\vec{\nabla}\vec{U} \cdot \vec{n} = 0$	$\vec{\nabla}k \cdot \vec{n} = 0$	$\vec{\nabla}\omega \cdot \vec{n} = 0$	calculated	$\vec{\nabla}p \cdot \vec{n} = 0$
Inlet	$(U_\infty,0,0)$	k_{inlet}	ω_{inlet}	calculated	$\vec{\nabla}p \cdot \vec{n} = 0$
Outlet	$\vec{\nabla}\vec{U} \cdot \vec{n} = 0$	$\vec{\nabla}k \cdot \vec{n} = 0$	$\vec{\nabla}\omega \cdot \vec{n} = 0$	calculated	0
Above	$\vec{U} \cdot \vec{n} = 0$	$\vec{\nabla}k \cdot \vec{n} = 0$	$\vec{\nabla}\omega \cdot \vec{n} = 0$	calculated	$\vec{\nabla}p \cdot \vec{n} = 0$

Table 2: Boundary conditions for the flat plate. OWF denotes a wall function for ω (OmegaWallFunction); SWF: SpaldingWallFunction (Spalding et al., 1961); and the calculated condition for ν_t assigns values at each boundary face by evaluating the model-specific ν_t equation.

These meshes present a notable challenge due to the small rounded leading edge, which requires intense local refinement ($y^+ < 1$) to capture the curvature without introducing excessive numerical diffusion or artifacts in the initial laminar separation. Three meshes were proposed for each case; for practical purposes, the intermediate mesh with 107,280 cells in 2D was used in this work, ensuring sufficient resolution for the development of ν_t from laminar conditions. The boundary conditions are summarized in Table 2.

4.2 NACA0025

This airfoil introduces aerodynamic complexity, where transition depends not only on Re_x but also on pressure gradients and curvature, potentially causing laminar separation on the up-

per (suction) surface. This case is relevant for low-Re applications (e.g., drones, UAVs), as separation reduces C_l and increases C_d; the models must capture how transition mitigates or exacerbates these effects, compared to surface C_p data.

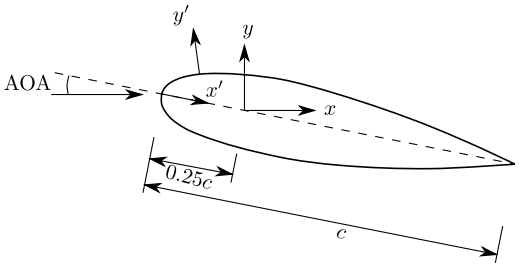

(a) Geometric schematic (AOA=5°, $c = 0.3$ m, $Re_c = 10^5$)

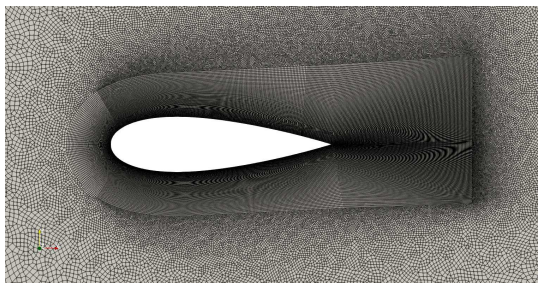

(b) Refined structured mesh ($y^+ < 0.4$ near the wall)

Figure 3: Representation of the NACA0025 airfoil and its numerical discretization.

Patch	$\vec{U}$ [m/s]	k [m^2/s^2]	ω [1/s]	ν_t [m^2/s]	p [m^2/s^2]
airfoil	$(0, 0, 0)$	0	OWF	SWF	$\vec{\nabla} p \cdot \vec{n} = 0$
inlet	$(4.9, 0.43, 0)$	2.4×10^{-5}	16.33	calculated	$\vec{\nabla} p \cdot \vec{n} = 0$
bottom	$(4.9, 0.43, 0)$	2.4×10^{-5}	16.33	calculated	$\vec{\nabla} p \cdot \vec{n} = 0$
top	$\vec{\nabla}\vec{U} \cdot \vec{n} = 0$	$\vec{\nabla} k \cdot \vec{n} = 0$	$\vec{\nabla}\omega \cdot \vec{n} = 0$	calculated	$\vec{\nabla} p \cdot \vec{n} = 0$
outlet	$\vec{\nabla}\vec{U} \cdot \vec{n} = 0$	$\vec{\nabla} k \cdot \vec{n} = 0$	$\vec{\nabla}\omega \cdot \vec{n} = 0$	calculated	0

Table 3: Boundary conditions for NACA0025. OWF denotes a wall function for ω (OmegaWallFunction); SWF: SpaldingWallFunction (Spalding et al., 1961); and the calculated condition for ν_t assigns values at each boundary face by evaluating the model-specific ν_t equation.

The meshes were generated in 2D using GMSH and custom Octave scripts for parameterization, employing a C-grid topology ($30\,c$ in the axial direction, $20\,c$ normal to the flow). Refined structured regions wrap the surface up to $0.3\,c$ and $0.7\,c$ downstream of the trailing edge, prioritizing $y^+ < 0.4$, a maximum growth rate of 1.02, and mesh alignment with the flow to capture vorticity and ensure numerical stability (see Fig. 3).

5 RESULTS

The results of the numerical simulations using the proposed models are presented below, comparing their performance with experimental data and theoretical correlations for the flat-plate (T3 series) and NACA0025 airfoil cases. This section analyzes the models' ability to predict laminar–turbulent transition, highlighting strengths, limitations, and applicability to aerodynamic flows.

5.1 Flat Plate (T3 Series)

The distributions of the skin friction coefficient (C_f) versus Re_x are shown in Fig. 4. For T3AM, with low Tu, the k-ω SSTLM model (Langtry et al., 2004) closely follows the laminar Blasius correlation (Blasius, 1907) up to $Re_x \approx 3 \times 10^5$, initiating transition in agreement

with experiments. In contrast, the γ SST model (Menter et al., 2015) predicts an earlier transition at $Re_x \approx 2.5 \times 10^5$, possibly due to overestimation of intermittency production under low-disturbance conditions, as observed in similar validations (Huang et al., 2023). The k-ω LowRe model (Wilcox, 1992) underestimates C_f during transition, being limited to fully turbulent flows.

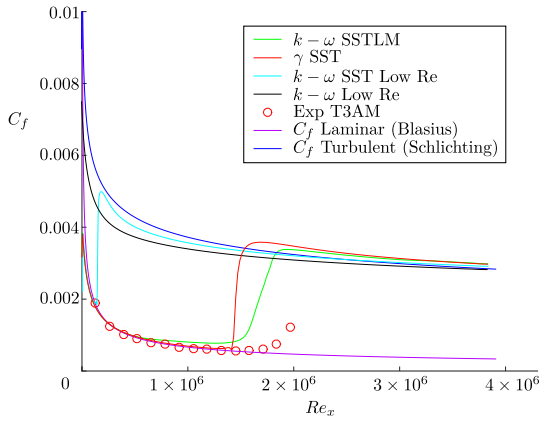

(a) T3AM ($Tu = 0.9\%$)

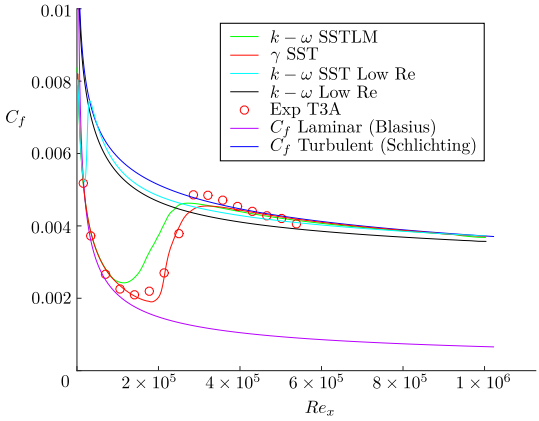

(b) T3A ($Tu = 3.3\%$)

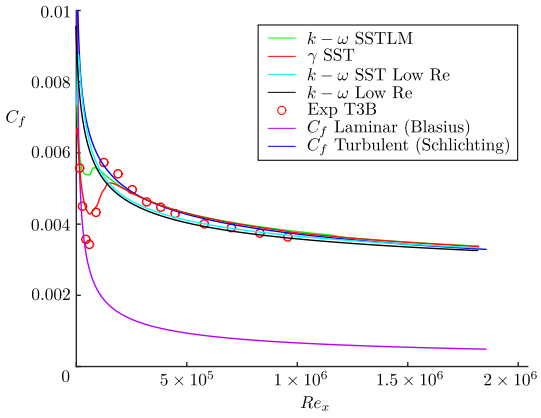

(c) T3B ($Tu = 6.5\%$)

Figure 4: C_f distributions versus Re_x for the T3 cases, comparing numerical models (k-ω SSTLM, γ SST, k-ω LowRe) with experimental data (Ryhming, 1990) and theoretical correlations (Blasius (1907), Schlichting and Gersten (2016)).

With increasing Tu (T3A and T3B), transition occurs earlier, consistent with instability mechanisms amplified by free-stream turbulence Schlichting and Gersten (2016). In T3B, k-ω SSTLM predicts the onset of turbulence around $Re_x \approx 2 \times 10^5$, with a relative error <5% compared to ERCOFTAC data. Here, γ SST performs better, aligning more closely thanks to its γ equation, which initially dampens ν_t. All models smooth the C_f jump during transition, a common RANS artifact compared to DNS.

Fig. 4 confirms the robustness of k-ω SSTLM for Tu values of $0.9 - 3.3\%$ (Fig. 4a and 4b), but for high Tu (Fig. 4c), γ SST stands out, consistent with recent findings recommending additional calibration of γ production for accelerated flows (Huang et al., 2023). This underscores the need for leading-edge correction terms to enhance generality in industrial applications.

5.2 NACA0025 Airfoil

For the NACA0025 at $Re_c = 10^5$ and AOA = 5°, adverse pressure gradients on the suction side induce laminar separation, testing the models' sensitivity to curvature and pressure variations (Ziadé et al., 2018). The C_p distributions versus x/c (Fig. 5) assess how transition affects the surface pressure distribution and stall onset, with emphasis on post-separation reattachment prediction.

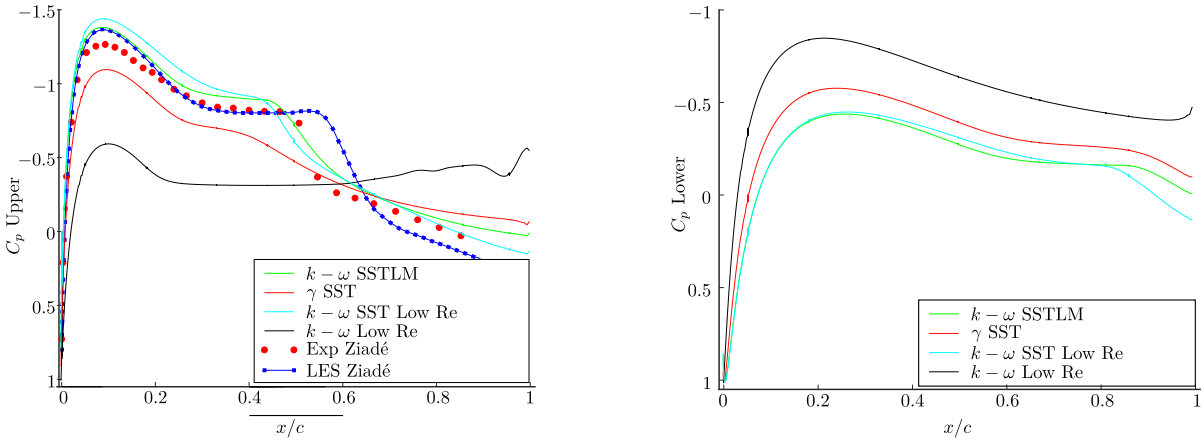

(a) Upper surface

(b) Lower surface

Figure 5: Comparison of C_p versus x/c for NACA0025, showing RANS models (k-ω SSTLM, γ SST, k-ω LowRe) against experimental and LES data (Ziadé et al., 2018).

On the upper surface, the k-ω SSTLM and k-ω SSTLowRe models predict a suction peak at $x/c \approx 0.08$, with values similar to LES results (Ziadé et al., 2018), although slightly overestimating the peak magnitude (5–7%). The collapse of boundary layer separation occurs at $x/c \approx 0.45$ for both models, showing a small offset relative to the experimental data ($x/c \approx 0.47$), indicating a moderately accelerated transition. In contrast, γ SST and k-ω LowRe also locate the peak at $x/c \approx 0.08$, but differ in recovery: γ SST leads to premature reattachment due to its low initial suction and overproduction of intermittency, while k-ω LowRe, designed for fully turbulent flows, fails to achieve subsequent reattachment, resulting in a fully separated boundary layer (deviation >10% vs. LES). This limitation highlights the need for laminar-region calibration for low-Re_c airfoils, as observed in recent validations (Huang et al., 2023).

On the lower surface, where the pressure gradient is favorable and no experimental data is available for this regime, all models show a fully attached boundary layer, with smooth C_p distributions dependent on the resolution on the upper surface. The pressure asymmetry limits the overall aerodynamic performance of the airfoil, emphasizing how suction-side failures propagate to total lift (C_l) and drag (C_d).

Property	k-ω **SSTLM**	γ **SST**	k-ω **SSTLowRe**	k-ω **LowRe**
C_d	9.947×10^{-2}	1.18×10^{-1}	7.261×10^{-2}	1.883×10^{-1}
C_l	8.236×10^{-1}	3.259×10^{-1}	8.328×10^{-1}	-5.79×10^{-1}

Table 4: Integrated coefficients for NACA0025 at $Re_c = 1 \times 10^5$ and AOA = 5°

The integrated aerodynamic coefficients, estimated from the C_p distributions via numerical

integration, are presented in Table 4. These values reflect the differences among models. The absence of experimental data on the lower surface limits direct validation, but trends suggest that k-ω SSTLM and k-ω SSTLowRe adequately predict the behavior of this airfoil in this regime.

6 CONCLUSIONS

This work evaluated several RANS models for predicting laminar–turbulent transition over flat plates and airfoils, with emphasis on their performance against benchmark cases such as the ERCOFTAC T3 series and the NACA0025 airfoil. The results show that the k–ω SSTLM and γ–SST models provide robust predictions of the skin friction coefficient (C_f) on flat plates under various levels of free-stream turbulence, showing good agreement with classical correlations by Blasius and Schlichting. Although the exact location of transition does not perfectly match experimental data, this discrepancy has a limited impact on the overall solution. Considering the intrinsic complexity of modeling transition and the low computational cost of these models compared to LES or DNS simulations, their results can be considered satisfactory for preliminary design studies.

The k–ω LowRe and k–ω SSTLowRe models perform adequately in fully turbulent flows, showing errors comparable to SSTLM in post-transition regions, as reported in Cortes and Marquez Damián (2023, 2024). However, they exhibit significant limitations in predicting the initial laminar phase, prematurely triggering transition and amplifying errors in cases where the laminar region is relevant, such as T3AM and T3A. This indicates that these models are appropriate when the laminar phase is secondary but are not recommended for configurations sensitive to transition, such as low-Reynolds-number airfoils or flat plates with low inlet turbulence, where the laminar region occupies a substantial portion of the domain.

For airfoils, such as the NACA0025 at $Re_c = 10^5$ and AOA = 5°, the k–ω SSTLM model provides a reasonable approximation of the maximum suction magnitude and improves the prediction of laminar separation collapse. The k–ω SSTLowRe model, despite its simplicity, achieves a similar boundary layer reattachment as that of SSTLM, since this zone is not affected by the additional SSTLM transport variables. However, it exhibits a larger error in the peak suction magnitude, being more sensitive to laminar effects and the onset of transition. The γ SST model, in contrast, overestimates turbulent viscosity on the upper surface, resulting in locally increased velocity and pressure and adversely affecting aerodynamic performance, although it correctly captures the position of separation collapse. Finally, k–ω LowRe, designed for fully turbulent flows, fails to represent the laminar region on the upper surface, resulting in a completely separated boundary layer without reattachment, which limits its applicability in this regime.

In summary, while the evaluated models provide reasonable approximations under controlled conditions, their generalization is limited by inherent simplifications in their transport equations and treatment of transition. Although suitable for academic studies and preliminary design, their application to complex geometries or industrial conditions requires additional calibration. This study shows that RANS models capture global trends but cannot substitute detailed, computationally intensive LES/DNS analyses for precise transition studies.

7 ACKNOWLEDGEMENTS

The authors acknowledge the funding provided by ANPCyT through project PICT-2018-03106 "Computational simulation of turbulent particulate flows applied to fluid-solid and fluid-

fluid systems." We also recognize the contributions of the developers and communities associated with OpenFOAM®, Octave, Inkscape, and Paraview®. This work is part of project PID-UTN-8685 "Numerical methods for low Reynolds number flows with applications in civil and mechanical engineering."

REFERENCES

Anderson J.D. *Fundamentals of Aerodynamics*. McGraw-Hill, 5th edition, 2010.

Blasius H. *Grenzschichten in Flüssigkeiten mit kleiner Reibung*. Druck von BG Teubner, 1907.

Cortes F.L. and Marquez Damián S. Evaluación de modelos turbulentos para la obtención del perfil energía cinética turbulenta. flujo en placa plana. *Mecánica Computacional*, 40(10):413–422, 2023.

Cortes F.L. and Marquez Damián S. Modificación del modelo k-omega sst para la obtención del perfil de energía cinética turbulenta: Flujo en placa plana. *Mecánica Computacional*, 41(6):333–341, 2024. http://doi.org/10.70567/mc.v41i6.33.

ERCOFTAC. Ercoftac classic database - flat plate t3 series. Technical Report, European Research Community on Flow, Turbulence and Combustion, 1995.

Fürst J. gammasst: A three-equation transition and turbulence model for OpenFOAM. https://github.com/furstj/gammaSST, 2023. Accedido: 2025-09-13. Basado en Menter et al. (2015).

Huang X., Li Y., and Wang Z. Revisiting rans prediction of transitional flow on t3a flat plate subject to various freestream turbulences. *Computers & Fluids*, 252:105745, 2023. http://doi.org/10.1016/j.compfluid.2023.105810.

Langtry R.B., Menter F., Likki S., Suzen Y., Huang P., and Vo¨ lker S. A correlation-based transition model using local variables: Part ii—test cases and industrial applications. In *Turbo Expo: Power for Land, Sea, and Air*, volume 41693, pages 69–79. 2004. http://doi.org//10.1115/GT2004-53454.

Menter F.R., Langtry R.B., Likki S., Suzen Y.B., Huang P., and Völker S. A correlation-based transition model using local variables—part i: model formulation. *Journal of turbomachinery*, 128(3):413–422, 2006. http://doi.org//10.1115/1.2184352.

Menter F.R., Smirnov P.E., Liu T., and Avancha R. A one-equation local correlation-based transition model. *Flow, Turbulence and Combustion*, 95(4):583–619, 2015. http://doi.org/10.1007/s10494-015-9622-4.

Pope S.B. Turbulent flows. *Measurement Science and Technology*, 12(11):2020–2021, 2001. http://doi.org/10.1088/0957-0233/12/11/705.

Ryhming I. Testcase specifications. In D. Pironneau, W. Rode, and I. Ryhming, editors, *Numerical Simulation of Unsteady Flows and Transition to Turbulence*. ERCOFTAC, 1990. Part 1: Testcases T3A and T3B.

Schlichting H. and Gersten K. *Boundary-layer theory*. springer, 2016.

Spalding D. et al. A single formula for the law of the wall. *Journal of Applied Mechanics*, 28(3):455–458, 1961. http://doi.org/10.1115/1.3641728.

Wilcox D.C. The remarkable ability of turbulence model equations to describe transition. In *California State Univ., The Fifth Symposium on Numerical and Physical Aspects of Aerodynamic Flows*. 1992.

Ziadé P., Feero M.A., Lavoie P., and Sullivan P.E. Shear layer development, separation, and stability over a low-reynolds number airfoil. *Journal of Fluids Engineering*, 140(7):071201, 2018. http://doi.org/10.1115/1.4039233.